Supporting information

3D NiCoP flowers assembled by 2D carbon-coating nanosheets as efficient and stable positive electrode for supercapacitor

The contents of ESI

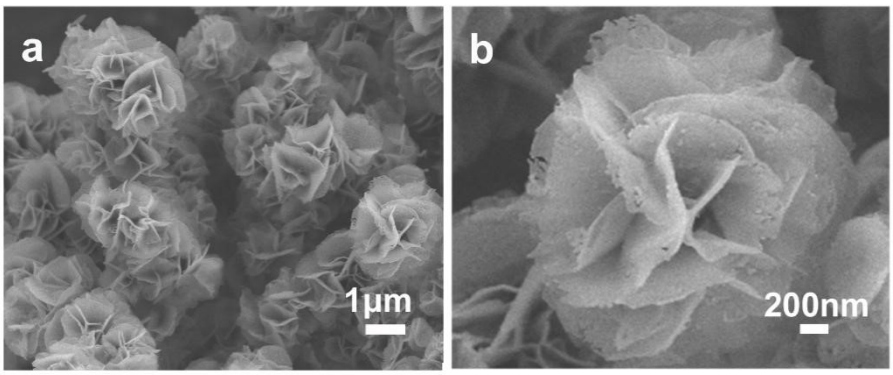

Figure S1. SEM images of NiCoP.

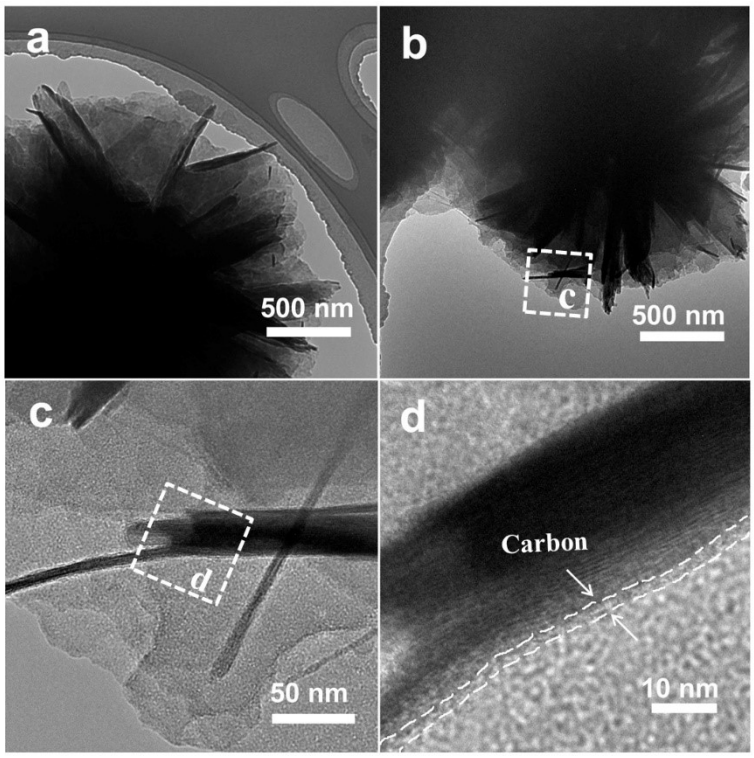

Figure S2. TEM images of (a) NiCo-OH precursor, (b-d) NiCo-OH/C-2.

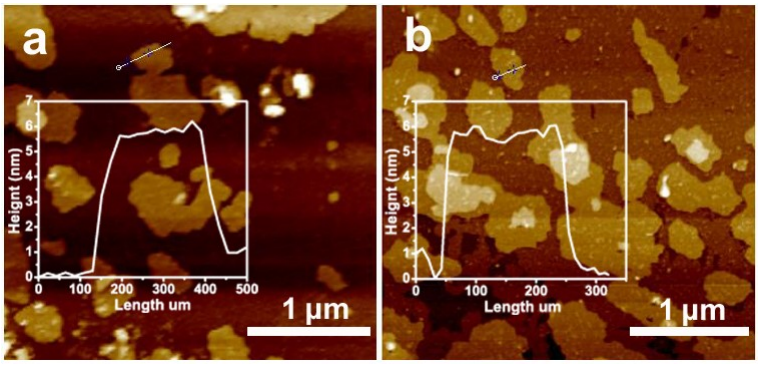

Figure S3. AFM image for (a)NiCo-OH/C-2, (b)NiCoP/C-2 and corresponding height profiles.

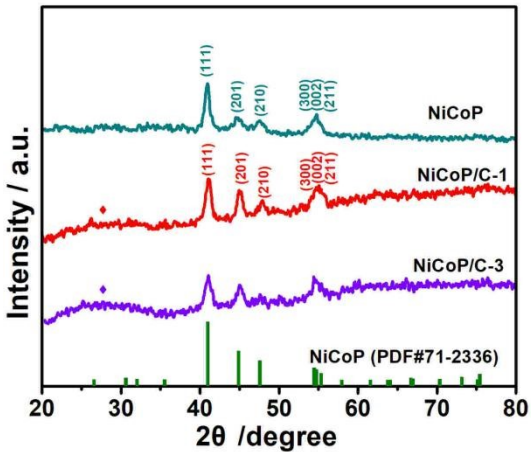

Figure S4. Typical XRD patterns of NiCoP, NiCoP/C-1 and NiCoP/C-3.

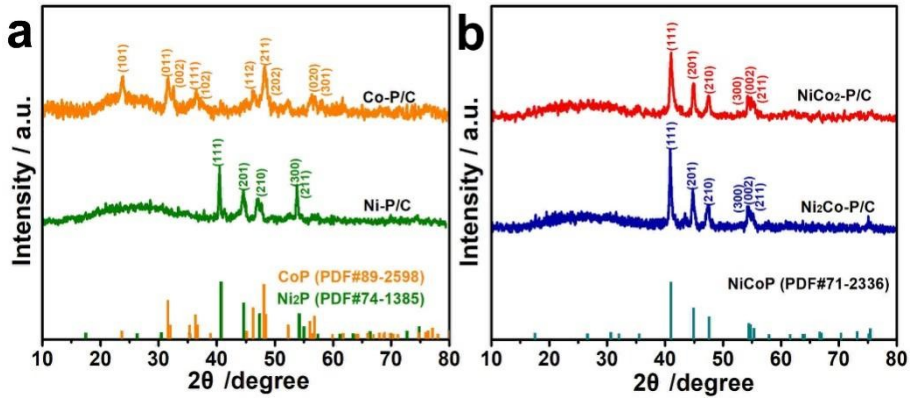

Figure S5. Typical XRD patterns (a)Co-P/C and Ni-P/C, (b)$NiCo_2P$/C and Ni_2CoP/C.

A series of other control samples were also fabricated by tuning the mol ratio of $Co(NO_3)_2{\cdot}6H_2O$ and $Ni(NO_3)_2{\cdot}6H_2O$ to 1 : 0, 0 : 1, 2 : 1 and 1 : 2, while maintaining a total molar amount of 18 mmol. The final carbon coated phosphating samples are marked as Co-P/C, Ni-P/C, $NiCo_2P$/C and Ni_2CoP/C(as shown in Table S3). In figure S5a, the peaks of Co-P/C located at 23.6°, 31.5°, 32.0°, 36.3°, 36.6°, 46.2°, 48.1°,48.4°,56.0° and 56.7° can be indexed to (101), (011), (002), (111), (102), (112), (211), (202), (020) and (301) planes of CoP (JCPDS no. 89-2598). The diffraction peaks of Ni-P/C is match well with the hexagonal Ni_2P (JCPDS no. 74-1385). The peaks located at 41.7°, 44.6°, 47.3°, 54.1°and 54.9°can be assigned to (111) (201), (210), (300) and (211) plane of Ni_2P, respectively. The results indicate that the Co-P/C and Ni-P/C samples are mainly composed of single metal CoP and Ni2P, respectively. For comparison, the molar ratios of cobalt and nickel sources have been tuned to $Co(NO_3)_2{\cdot}6H_2O$: $Ni(NO_3)_2{\cdot}6H_2O$ is 2 : 1 ($NiCo_2P$/C) and $Co(NO_3)_2{\cdot}6H_2O$: $Ni(NO_3)_2{\cdot}6H_2O$ is 1 : 2 (Ni_2CoP/C) (Figure S5b). The XRD of $NiCo_2P$/C and Ni_2CoP/C show similar pattern with that of NiCoP(JCPDS no. 71-2336), indicating that in the presence of both cobalt and nickel ions, the close ionic radii of cobalt and nickel ions facilitate the formation of a cobalt nickel 1:1 precursor, which in

turn generates NiCoP material. The $NiCo_2P$/C and Ni_2CoP/C samples are mainly composed of NiCoP.

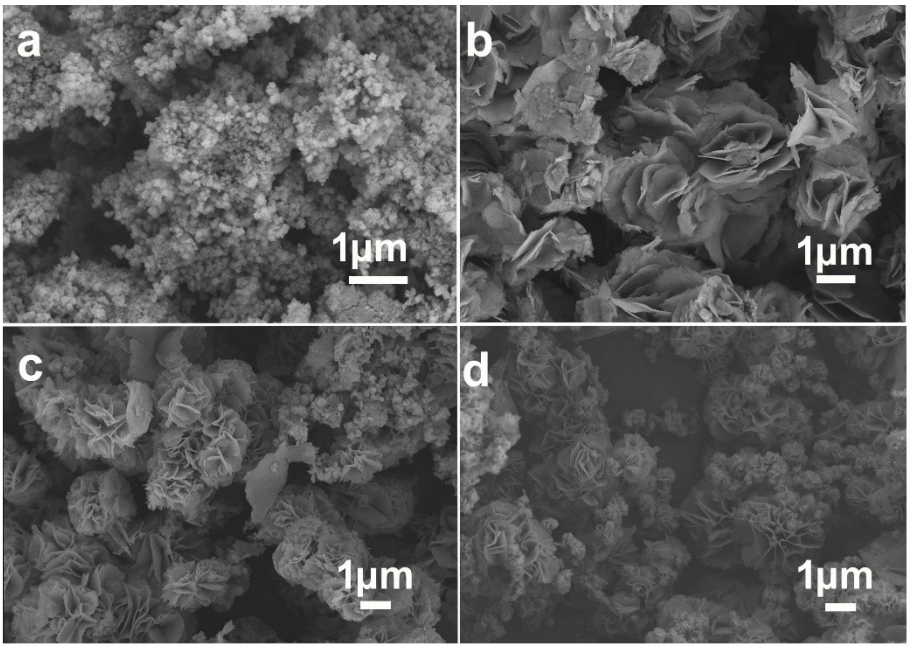

Figure S6. SEM images of (a)Co-P/C, (b)Ni-P/C, (c)$NiCo_2P$/C and (d)Ni_2CoP/C.

Figure S6 shows the SEM test results of Co-P/C, Ni-P/C, $NiCo_2P$/C and Ni_2CoP/C. Figure S6a shows Co-P/C composed of inhomogeneous nanoparticles, the nanoparticles are approximately several tens of nanometers in equivalent diameter. This tight structure is highly detrimental to the effective contact between the active material and the electrolyte. The SEM image of Ni-P/C shows a sheet-like morphology, the uniform nanosheets with a thickness of several tens of nanometers and a lateral size above micrometers. In the presence of both cobalt and nickel sources, the product exhibits a 3D flower like structure assembled by sheets. The density of the sheet-like petals in $NiCo_2P$/C is varies and it is accompanied by the appearance of particles. The flower-like structures shown in Figure S6d is non-uniform in size. By adjusting the cobalt nickel molar ratio, the material composition generated is similar, but there are some differences in morphology. By tuning the cobalt nickel molar ratio, we obtain optimal morphology sample NiCoP/C-2 with uniform morphology at cobalt nickel ratio is 1:1.

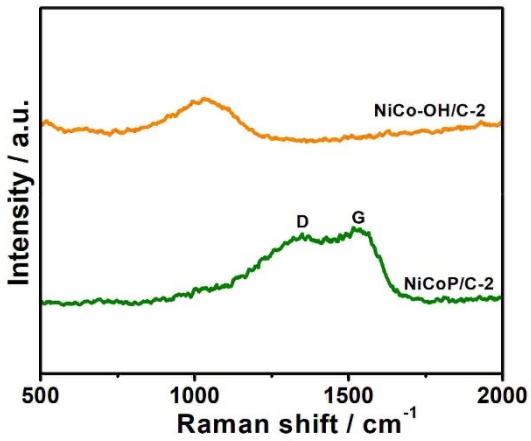

Figure S7.Raman spectrum of NiCo-OH/C-2 and NiCoP/C-2.

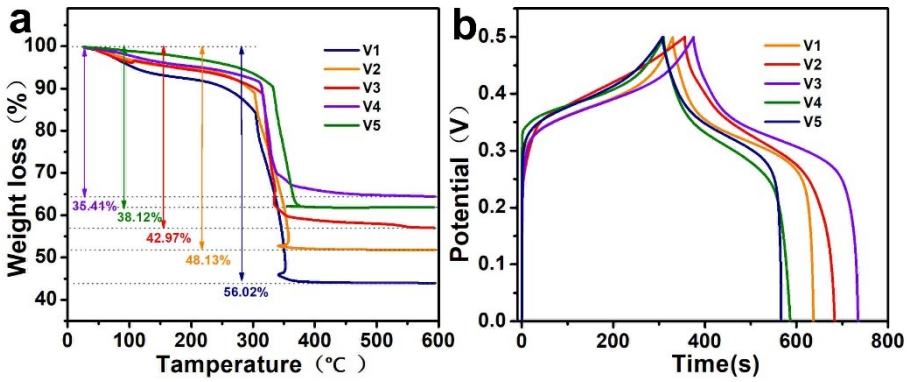

Figure S8. (a) TG curves and (b) GCD curves of V1, V2, V3, V4 and V5.

Figure S8a shows the TG curves of V1, V2, V3, V4 samples. As the ethanol volume increases in the synthesis conditions, the composite carbon content in lables V1, V2，V3, V4 and V5 are approximately 35.41 wt%, 38.12 wt%, 48.13 wt%and 56.02 wt%. In ethanol-water mixture, it was found that the ethanol-water ratio can regulate the carbon coating content of composite materials, and the water ethanol mixture (water 22 mL+ethanol 13 mL) can better disperse the precursor NiCo-OH in the solvent, ensuring the appropriate carbon coating quality of the precursor NiCo-OH. The GCD curves of V1, V2, V3, V4 and V5 are shown in Figure S8b, at 1A g^{-1}, the capacitance of V1, V2, V3, V4 and V5 are 619 Fg^{-1}, 652 Fg^{-1},719 Fg^{-1}, 553 Fg^{-1} and 519 Fg^{-1}, respectively, we found that the electrode material had the best capacitance performance under V3 synthesis solvent conditions. Therefore, we chose V3 as the optimal carbon coated solvent condition.

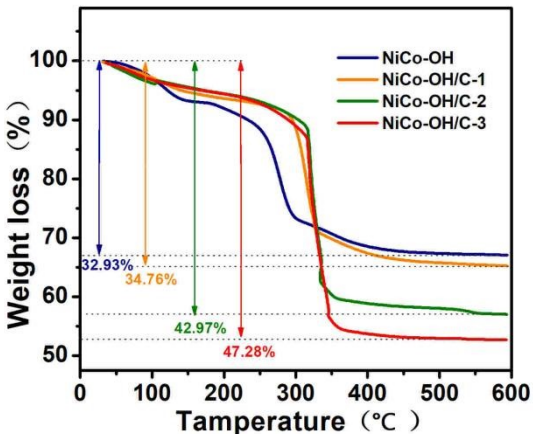

Figure S9. TG curves of NiCo-OH, NiCo-OH/C-1, NiCo-OH/C-2 and NiCo-OH/C-3.

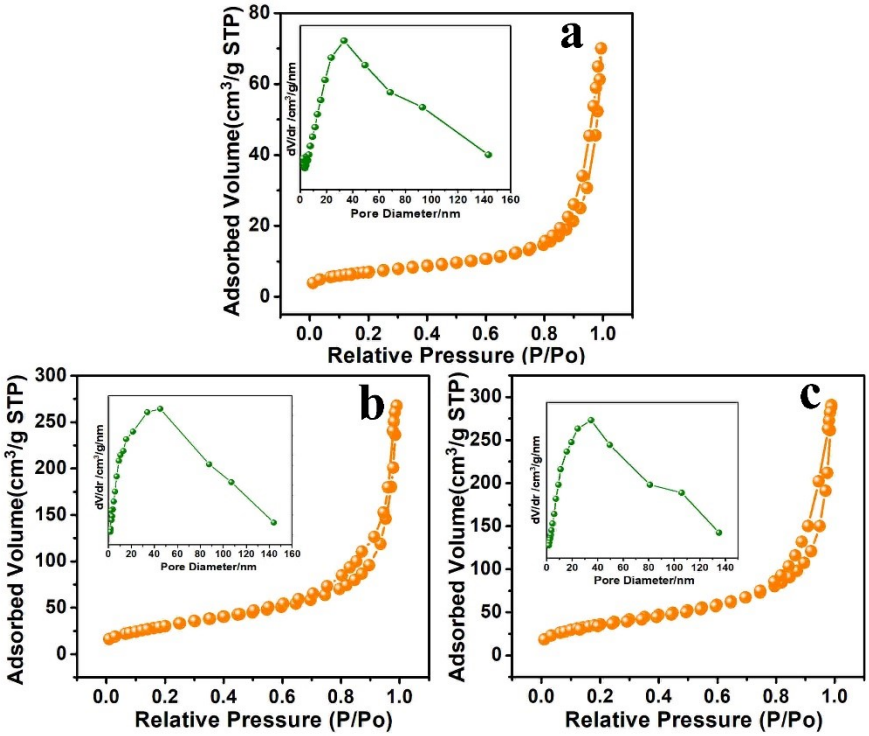

Figure S10. Nitrogen adsorption–desorption isotherm and the corresponding NLDFT PSD curves(inset) of NiCo-OH and Ni-P/C and Co-P/C.

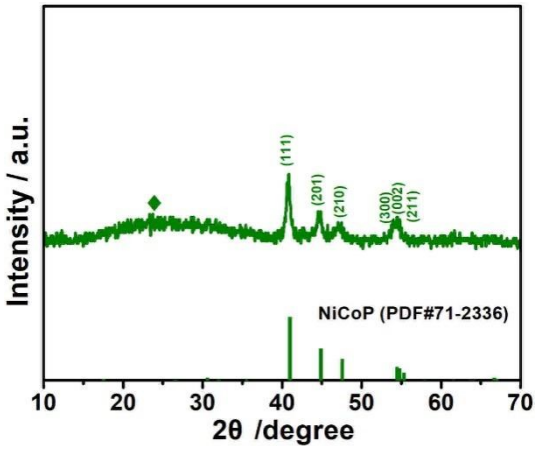

Figure S11. The XRD pattern of NiCoP/C-2 sample after three electrode testing.

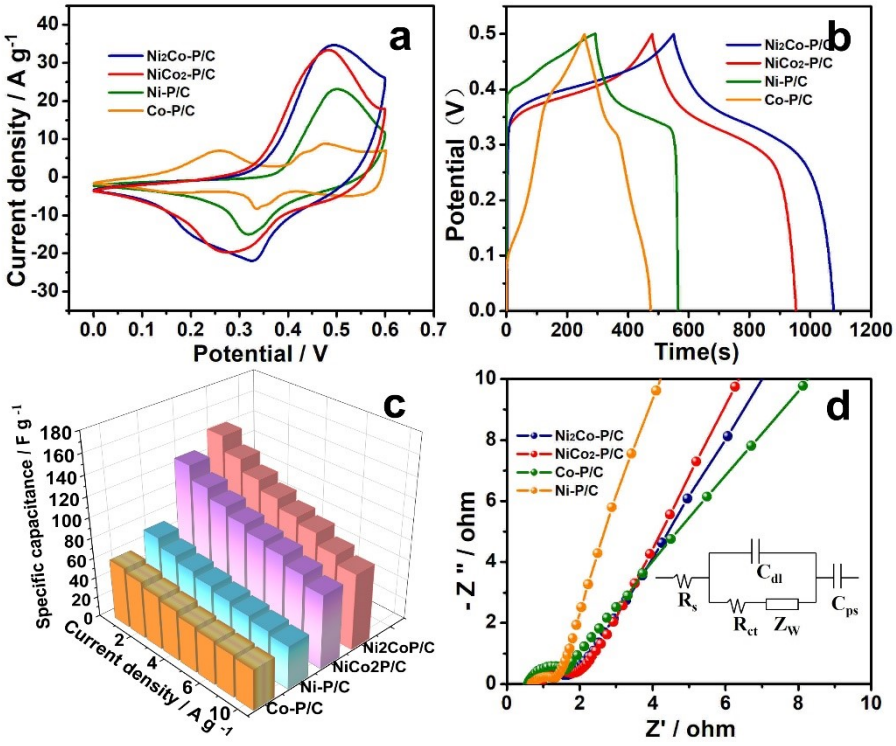

Figure S12. Electrochemical performance of Co-P/C, Ni-P/C, $NiCo_2P$/C and Ni_2CoP/C for supercapacitors:(a) CV curves at 10 mV s^{-1}; (b) Galvanostatic charge/discharge curves at a current density of 1 A g^{-1}. (c) The specific capacitances at different current densities; (d) The EIS curves (inset: an equivalent circuit based on the EIS curves).

Figure S12a shows CV image of Co-P/C, Ni-P/C, $NiCo_2P$/C and Ni_2CoP/C samples at a scan rate of 10 mV s^{-1}. All CV curves show different redox reaction peaks, this is main indicating electrodes' Faraday redox reaction behavior, the redox peak is mainly attributed to the reversible reaction of Co^{2+}/Co^{3+} and Ni^{2+}/Ni^{3+}. Figure S12b shows Co-P/C, Ni-P/C, $NiCo_2P$/C and Ni_2CoP/C samples' charge

and discharge time, Through the calculation of capacitance formulas C=I Δ t/ Δ mV, we obtained the capacitance values of Co-P/C, Ni-P/C, $NiCo_2P$/C and Ni_2CoP/C are 436 F g^{-1}, 540 F g^{-1}, 946 F g^{-1} and 1056 F g^{-1} respectively. The corresponding current-capacitance (F) values at different current density are calculated and shown in figure S12c, compared with other comparison sample, Ni_2CoP/C has slightly higher capacitance performance. Although the capacitance performance of single metal Co-P/C material is relatively low, but it has a significant advantage in rate performance, this is closely related to the basic characteristics of cobalt based materials. The electrochemical impedance spectroscopy (EIS) results for Co-P/C, Ni-P/C, $NiCo_2P$/C and Ni_2CoP/C are shown in figure S12d. According to fitting results, Rs, Rct, Cdl, Zw and Cps are the representative of the solution resistance, charge transfer resistance, double layer capacitance, diffusion resistance and pseudocapacitance, respectively. In the high-frequency region, the electrochemical impedance spectra of all samples exhibit nearly half circular arcs. In the low-frequency region, the sample spectra show oblique straight lines. Among them, electrode materials have a smaller arc radius and a smaller angle with the y-axis, resulting in lower internal resistance and higher charge transfer rate, making it suitable for use as an electrode material for supercapacitors.

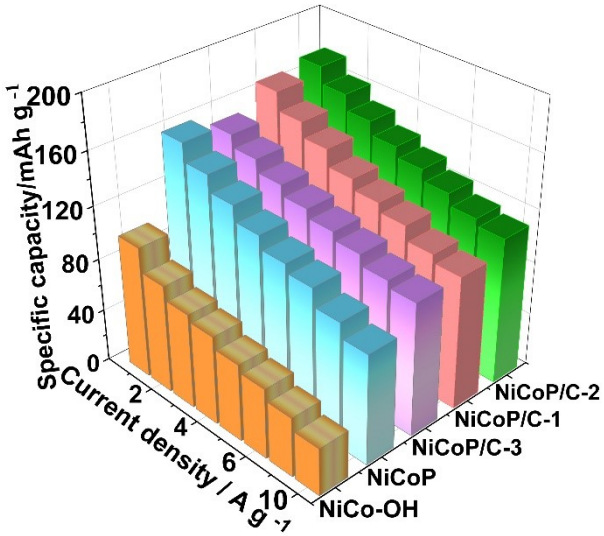

Figure S13. The specific capacity at 1-10 A g^{-1} of NiCo-OH, NiCoP, NiCoP/C-1, NiCoP/C-2 and NiCoP/C-3.

The specific capacity (mAh g^{-1}) calculated from the charge-discharge curve according to the formula: $Q = \frac{Q_{mA\,h}}{m} = \frac{I\,\Delta t}{m}$, Where I is discharge current(mA), Δt is discharge time(h) and m is the active material mass(g).

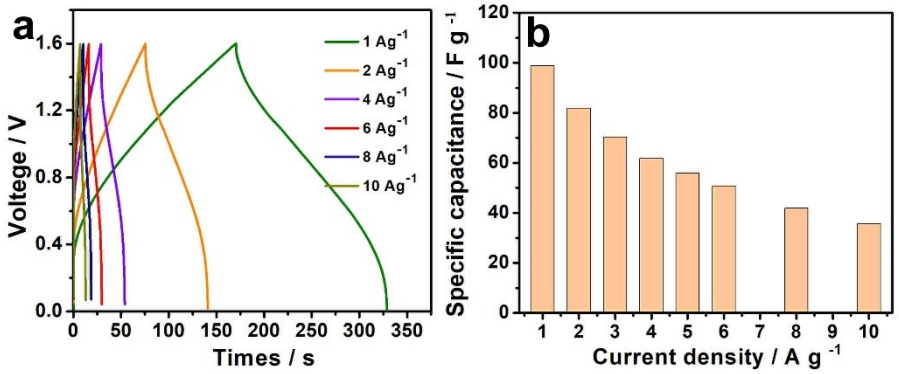

Figure S14. Electrochemical performances of the NiCoP//N-PC ASC device: (a) GCD curves; (b) The specific capacitances at different current densities.

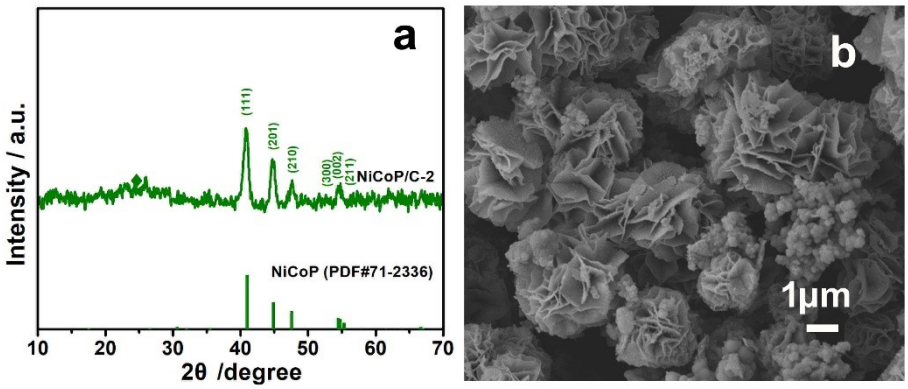

Figure S15. (a)XRD patterns and (b)SEM picture of the NiCoP/C-2 after 8000 GCD cycles.

Figure S15a shows the XRD pattern of the NiCoP/C-2 electrode material after 8000 cycles is almost identical to the XRD spectrum of Figure 3a, indicating that the crystal structure of the NiCoP/C-2 material remains relatively stable during the cycling process. After cycling, NiCoP/C-2 material did not undergo significant crystal phase transformation, structural damage or the formation of new phases and there is no significant irreversible chemical reactions occurred during the cycling process. It is prove that the physical and chemical properties of the NiCoP/C-2 electrode material can remain consistent during long-term cycling, and it has excellent cycling stability. Figure S15b shows the SEM image of the NiCoP/C-2 electrode material after 8000 GCD cycles. The morphology of NiCoP/C-2 material that flower-like structure assembled with nanosheets almost no significant changes, this proves that the structural stability of electrode materials is very good, which is very beneficial for the cycling performance of electrode materials. However, the SEM photos after GCD cycles was not clean, we can

see some clustered particles, this may be due to residual additives added during electrode preparation.

Table S1. The synthesis conditions for different hydrothermal precursor.

Sample	$Ni(NO_3)_2$ （mmol）	$Co(NO_3)_2$ （mmol）	NaAc (mmol)	Hydrothermal Temperature (℃)
NiCo-OH	9	9	18	120 °C
Ni_2Co-OH	12	6	18	120 °C
$NiCo_2$-OH	6	12	18	120 °C
Ni-precusor	18	--	18	120°C
Co-precusor	--	18	18	120°C

Table S2. Different carbon coated precursor under different water-ethanol volume ratio.

Lables	Ni or Co Precursor (g)	glucose (g)	urea (g)	V_{Water}+ $V_{ethanol}$ (mL)	Hydrothermal Temperature (℃)
V1	0.1	0.3	1	35 + 0	160 °C
V2	0.1	0.3	1	30 + 5	160 °C
V3	0.1	0.3	1	22 + 13	160 °C
V4	0.1	0.3	1	15 + 20	160 °C
V5	0.1	0.3	1	0 + 35	160 °C

Table S3. The synthesis conditions for NiCo-OH/C and phosphide sample.

Sample	Ni or Co Precursor (g)	glucose (g)	urea (g)	Hydrothermal Temperature (℃)	Phosphating Temperature (℃)
NiCo-OH/C-1	0.1	0.1	1	160 °C	--
NiCo-OH/C-2	0.1	0.3	1	160 °C	--
NiCo-OH/C-3	0.1	0.5	1	160 °C	--
NiCoP/C-1	0.1	0.1	1	160 °C	300 °C
NiCoP/C-2	0.1	0.3	1	160 °C	300 °C
NiCoP/C-3	0.1	0.5	1	160 °C	300 °C

Ni_2Co-P/C	0.1	0.3	1	160 °C	300 °C
$NiCo_2$-P/C	0.1	0.3	1	160 °C	300 °C
NiCoP	0.1	--	--	--	300 °C
Ni-P/C	0.1	0.3	1	160 °C	300 °C
Co-P/C	0.1	0.3	1	160 °C	300 °C

Table S4. Textual parameters of all the as-prepared materials.

Sample	S_{BET} (m^2g^{-1})	Pore volume (cm^3g^{-1})	Pore size (nm)
NiCoP/C-2	120.96	0.62	25.14
NiCo-OH	24.79	0.11	18.73
NiCoP	63.27	0.28	16.62
Ni-P/C	116.3	0.46	16.41
Co-P/C	99.7	0.36	15.9

Table S5. The specific capacitance at different current densities for phosphide samples in our work.

Sample	C ($F g^{-1}$)							
	1A g^{-1}	2A g^{-1}	3A g^{-1}	4A g^{-1}	5A g^{-1}	6A g^{-1}	8A g^{-1}	10A g^{-1}
NiCoP	1157	1060	972	890	820	775	680	601
NiCoP/C-2	1261	1167	1084	1012	957	897	834	799
Co-P/C	436	410	381	360	330	313	301	290
Ni-P/C	540	480	441	410	380	355	330	307
NiCoP/C-1	1220	1121	1041	950	893	845	768	710
NiCoP/C-3	1095	1030	963	907	861	819	761	726
Ni_2Co-P/C	1056	951	866	798	735	692	609	545
$NiCo_2$-P/C	946	850	783	727	681	649	591	526